KINETIC INVESTIGATION ON STEAM GASIFICATION OF CHARCOAL UNDER DIRECT HIGH FLUX IRRADIATION

R. Müller, P. von Zedtwitz (ETH Zürich), A. Wokaun, A. Steinfeld (ETHZ and PSI)

The reaction kinetics of steam-gasification of coal are investigated for a quartz tubular reactor containing a fluidized bed directly exposed to concentrated solar radiation. Rate laws are formulated based on elementary reaction mechanisms describing reversible adsorption/desorption processes and irreversible surface chemistry. High quality syngas containing an equimolar mixture of H_2 and CO, and less than 5% CO_2, was produced at above 1400 K. The advantages of using concentrated solar radiation source for supplying high-temperature process heat are three-fold: 1) the calorific value of the fuel is upgraded; 2) the gaseous products are not contaminated by combustion by-products; and 3) emission of greenhouse gases is avoided.

1 INTRODUCTION

Hybrid solar/fossil endothermic processes, in which fossil fuels are used exclusively as the chemical source for H_2 production, and solar radiation as the energy source of high-temperature process heat, offer viable and efficient routes for fossil fuel decarbonization and CO_2 mitigation. The gasification of carbonaceous materials and related reactions have been performed using solar energy in exploratory early studies [1 and literature cited therein].

The steam-gasification of coal is a complex process, but the overall chemical conversion can be represented by the simplified net reaction:

$$C_1H_xO_y + (1-y)H_2O = (0.5x+1-y)H_2 + CO \qquad (1)$$

where x and y are the elemental molar ratios of H/C and O/C in coal, respectively, e.g. x= 0.43, y=0.03 for anthracite, x=0.81, y=0.23 for lignite. The thermodynamics of reaction (1) have been examined in [2]. This note presents a reaction kinetics study on the steam gasification of coal when the reactants are directly exposed to concentrated radiation [1]. The kinetics information, along with the thermodynamic characteristics, establishes the constraints to be imposed on the design and efficient operation of the solar chemical reactor.

2 EXPERIMENTAL SETUP

The chemical reactor consisted of a 25 mm-diameter, 25 cm-height quartz tube containing a coal/steam fluidized bed directly exposed to high flux irradiation. Tests were conducted at the ETH's high-flux solar simulator [3], using the experimental set-up depicted in Figure 1.

mean diameter	1 mm
bulk density	530 kg/m^3
apparent density (pellet)	815 kg/m^3
total specific surface	~1100 m^2/g
external specific surface	56 cm^2/g
total pore volume	0.78 ml/g

Table 1: Mean properties of activated charcoal pellets used as reactants in this study.

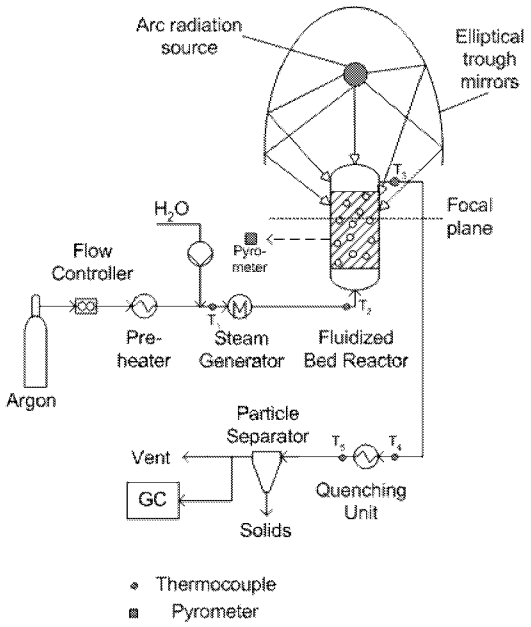

Fig. 1: Set-up at ETH's High-Flux Solar Simulator.

All experiments were conducted with activated charcoal (Norit, type RB1, derived from peat) in the form of pressed pellets of Geldart Group D type, with mean properties listed in Table 1. For typically Re_P~70, Sh_P~56, and Nu_P~8, the heat and mass transfer coefficients are h ~200 W/m^{2}K and k_m~0.6 m/s.

3 REACTION MECHANISM

Two distinct phenomena are considered [4]:

1. Reversible sorption of gaseous species onto the carbon surface,

$$H_2O_{(g)} + 2\Theta_V \underset{k_{-1}}{\overset{k_1}{\rightleftarrows}} \Theta_{OH} + \Theta_H \qquad (2)$$

$$CO_{(g)} + \Theta_V \underset{k_{-2}}{\overset{k_2}{\rightleftarrows}} \Theta_{CO} \qquad (3)$$

$$CO_{2(g)} + \Theta_V \underset{k_{-3}}{\overset{k_3}{\rightleftarrows}} CO_{(g)} + \Theta_O \qquad (4)$$

$$H_{2(g)} + \Theta_V \underset{k_{-4}}{\overset{k_4}{\rightleftarrows}} \Theta_{H_2} \qquad (5)$$

where, Θ_i represents the fraction of active carbon sites occupied by species i, and Θ_V is the fraction of vacant sites.

2. Irreversible reactions among adsorbed species and with molecules in the gas phase, described by:

$$\Theta_{OH} + \Theta_H \xrightarrow{k_5} \Theta_O + \Theta_{H_2} \quad (6)$$

$$\Theta_O + nC_i \xrightarrow{k_6} CO_{(g)} + n\Theta_V \quad (7)$$

$$CO_{2,(g)} + \Theta_{CO} \xrightarrow{k_7} 2CO_{(g)} + \Theta_O \quad (8)$$

where C_i are inactive carbon sites. Assuming steady state and balancing production/consumption of surface species leads to a system of linear equations, formulated in terms of complex rate constants K_i,

$$r_{H_2O} = -K_1 p_{H_2O} \quad (9)$$

$$r_{H_2} = K_1 p_{H_2O} \quad (10)$$

$$r_{CO} = K_1 p_{H_2O} + 2K_2 p_{CO_2} - 2K_1 K_3 p_{H_2O} p_{CO} \quad (11)$$

$$r_{CO_2} = -K_2 p_{CO_2} + K_1 K_3 p_{H_2O} p_{CO} \quad (12)$$

where $K_1=k_1k_5/(k_1+k_5)$, $K_2=k_3$, and $K_3=k_{-3}/k_6$. Mass balance for each species i over a differential surface element along the reactor axis yields,

$$d\dot{n}_i = r_i \, dA = r_i \, a \, dM_{Coal} \quad (13)$$

where r_i are the reactions rates defined by Eq. (9)-(12). The system of four coupled differential equations is solved numerically by Runge-Kutta by iterating on the values of K_i to minimize the difference between theoretically calculated and experimentally measured molar flow rates of products.

4 RESULTS

Figure 2 shows the theoretically modeled vs. the experimentally measured product flow rates for the four relevant species: The solid line represents perfect match. The root mean square deviation (RMS) is 0.99 for H_2O, CO, and CO_2, and 0.97 for H_2.

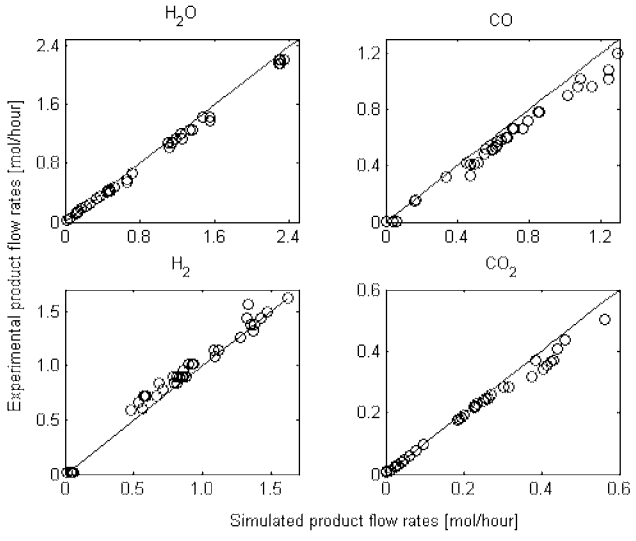

Fig. 2: Experimentally measured vs. theoretical modelled product flow rates.

The temperature dependence of each K_i is determined by imposing an Arrhenius-type rate law. The apparent activation energies and corresponding frequency factors are listed in Table 2. Parameter a is the mass specific surface area, in m^2/g. Since the K_i represent complex reaction mechanisms rather than elementary steps, a negative value for the apparent activation energy, as in the case of $E_{A,3}$, does not necessarily imply inconsistency with the transition state theory. Rather, it implies that E_A of the elementary reaction rate k_6 has to be higher than the one for k_{-3}. The activation energy obtained for K_1 is in good agreement with the values reported in [4], whereas the other activation energies obtained cannot be directly compared with previous work.

	$E_{A,i}$	*Frequency factor*	*RMS*
K_1a	174 kJ/mol	3.7 mol / (gsPa)	0.88
K_2a	-10.9 kJ/mol	$4.4*10^{-8}$ mol / (gsPa)	0.82
K_3	-169 kJ/mol	$7.3*10^{-12}$ Pa^{-1}	0.85

Table 2: Arrhenius kinetics parameters.

The gas product composition measured by GC is shown in Figure 3. Omitted is excess steam, which has been condensed downstream. Above 1300 K, the syngas mixture consists primarily of an equimolar mixture of H_2 and CO, as predicted by thermodynamic equilibrium. The CO_2 content is less than 5%. This syngas quality is notably superior than the one typically obtained in autothermal reactors, besides the additional benefit of the upgraded calorific value. The LHV (low heating value) of the products, assuming complete conversion, is 530 kJ/mol and 34% higher than that of the original feedstock.

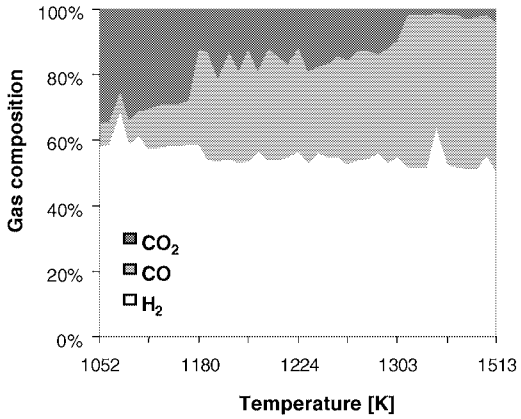

Fig. 3: Variation of the product gas composition (measured by GC) as a function of the fluidized bed temperature.

5 ACKNOWLEDGMENT

We gratefully acknowledge the financial support of the Swiss Federal Office of Energy.

6 REFERENCES

[1] R. Müller, P. von Zedtwitz, A. Wokaun, A. Steinfeld, Chem. Eng. Sci. **58**, 5111-5119 (2003).

[2] P. von Zedtwitz, A. Steinfeld, Energy **28**, 441-456 (2003).

[3] D. Hirsch, P. von Zedtwitz, T. Osinga, J. Kinamore, A. Steinfeld, J. Solar Energy Engng **125**, 117-120 (2003).

[4] H.J. Mühlen, *Zum Einfluss der Produktgase auf die Kinetik der Wasserdampfvergasung in Abhängigkeit von Druck und Temperatur*, Diss., Universität Essen (1983).